Structural Engineering and Mechanics, Vol. 9, No. 1 (2000) 37-50
DOI: http://dx.doi.org/10.12989/sem.2000.9.1.037

Analysis of orthotropic circular disks and rings under diametrical loadings

Takashi Tsutsumi†

Department of Civil Engineering, Fukushima National College of Technology, Iwaki, Fukushima 970-8034, Japan

Ken-ichi Hirashima‡

Department of Civil and Environmental Engineering, Yamanashi University, Kofu, Yamanashi 400-8511, Japan

Abstract. Very few studies on orthotropic circular disks or rings under diametrical loadings are conducted because of difficulties in treatment. This paper shows analytical solutions and gives the distributions of stresses and displacements by using Lekhnitskii's complex variable method. Several numerical results are shown by graphical representation.

Key words: orthotropy; elasticity; circular disk; circular ring; concentrated force.

1. Introduction

The diametral compression test is a simple and relatively inexpensive test means of measuring the tensile strength of brittle materials. This test is perfomed by placing a circular disk or cylinder between two (rigid) plates and applying a diametrical compressive load. The test induces a biaxial stress state in which the stress at the center of the disk is compressive in x-direction (σ_x), and tensile in the y-direction (σ_y). Theoretically, for an isotropic material, the tensile stress reaches a maximum on the vertical line along the disk center (i.e., at $x = 0$), except near the applied load, the stress has a constant magnitude of $P/\pi R$, where P is the applied load and R is the radius of the disk. Because for many brittle materials tensile strength is smaller than compressive strength, the material fails first in tension.

Circular plane problems, for orthotropic material under diametral compression were addressed by Cauweleart *et al.* (1994), Lemmon *et al.* (1996) and Lekhnitskii (1968); Cauweleart *et al.* obtained a solution using the theoretical results for a semi-finite plate under concentrated force. Lemmon *et al.* evaluated stresses and displacements using the finite element method, in which the applied load areas are very narrow. Lekhnitskii attempted to obtain the solution using complex variables: however, he was unable to obtain the displacement field because of the lack of equations for boundary conditions.

† Research Associate
‡ Professor

For the isotropic ring problem under diametral compression, Durelli *et al.* (1986) estimated stresses and displacements on the boundary using Nelson's formula. Hayashi (1960) obtained the stress fields for the orthotropic circular ring problem, but did not refer to cases under diametral compression.

In this paper, numerical results are presented for orthotropic circular plates under diametrical loadings. Further, by superposing solutions of orthotropic circular plates and orthotropic infinite plates with circular openings, numerical results are presented for orthotropic circular rings.

2. Fundamental equation

Consider a two-dimensional circular plate and circular ring which have an angle Ψ between the principal material direction and coordinate axis, as presented in Fig.1. The resultant force X_n, Y_n on the boundary in x, y-direction is represented using stress components:

$$\left.\begin{aligned} X_n &= \sigma_x \cos(n, x) + \tau_{xy} \cos(n, x) \\ Y_n &= \tau_{xy} \cos(n, x) + \sigma_y \cos(n, y) \end{aligned}\right\} \tag{1}$$

where

$$\cos(n, x) = \mp\frac{dy}{ds}, \quad \cos(n, y) = \pm\frac{dx}{ds} \tag{2}$$

s represents the length along the boundary of the infinitesimal element, the double sign follows the underside on the boundary of the circular plate, and the upper side on the inner boundary of the circular ring, respectively. If X_n and Y_n are known, the complex functions Φ_k (z_k) to obtain stresses and displacements are

$$\left.\begin{aligned} 2Re[\mu_1 \Phi_1(z_1) + \mu_2 \Phi_2(z_2)] &= \mp\int_0^s X_n ds \\ 2Re[\Phi_1(z_1) + \Phi_2(z_2)] &= \pm\int_0^s Y_n ds \end{aligned}\right\} \tag{3}$$

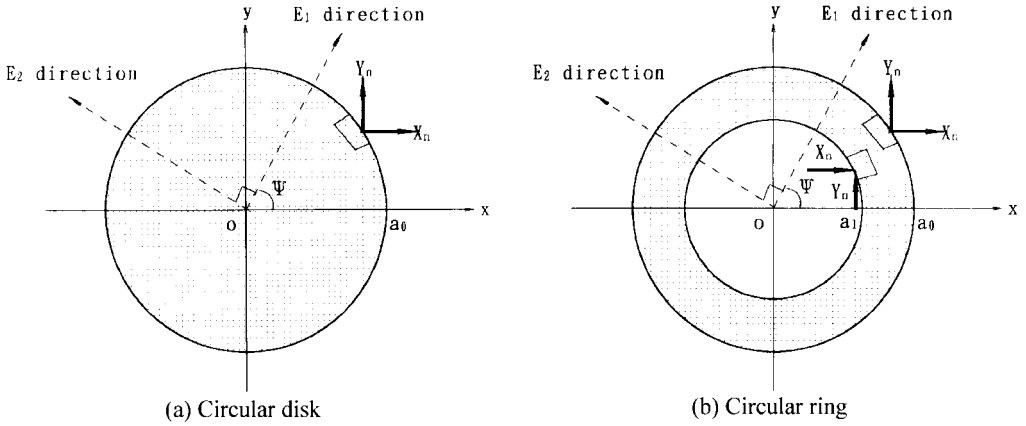

(a) Circular disk (b) Circular ring

Fig. 1 Tractions on the boundary

Now, the stress components σ_x, σ_y, τ_{xy} and displacement components u_x, u_y are given by

$$\left.\begin{aligned}\sigma_x &= 2Re[\mu_1^2\Phi'_1(z_1)+\mu_2^2\Phi'_2(z_2)]\\ \sigma_y &= 2Re[\Phi'_1(z_1)+\Phi'_2(z_2)]\\ \tau_{xy} &= -2Re[\mu_1\Phi'_1(z_1)+\mu_2\Phi'_2(z_2)]\end{aligned}\right\} \tag{4}$$

$$\left.\begin{aligned}u_x &= 2Re[p_1\Phi_1(z_1)+p_2\Phi_2(z_2)]-\omega_0 y+u_x^0\\ u_y &= 2Re[q_1\Phi_1(z_1)+q_2\Phi_2(z_2)]+\omega_0 x+u_y^0\end{aligned}\right\} \tag{5}$$

$$\left.\begin{aligned}p_1 &= a_{11}\mu_1^2+a_{12}, \qquad p_2 = a_{11}\mu_2^2+a_{12}\\ q_1 &= (a_{12}\mu_1^2+a_{22})/\mu_1, \quad q_2 = (a_{12}\mu_2^2+a_{22})/\mu_2\end{aligned}\right\} \tag{6}$$

Where *Re* represents the real part of the complex function in brackets; and u_x^0, u_y^0, and ω_0, represent the terms of rigid displacement and rigid rotation, respectively. And μ_1, μ_2 in the above equations are obtained as complex values of the characterestic equation below:

$$a_{11}\mu^4+(2a_{12}+a_{66})\mu^2+a_{22} = 0 \tag{7}$$

Where a_{11}, a_{12}, a_{22}, a_{66} are elastic constants, which are obtained using the elastic moduli E_1, E_2, shear elastic modulus G_{12} and poisson's ratio v_{12}, v_{13}, v_{31}, v_{23}, v_{32} at plane strain:

$$\left.\begin{aligned}a_{11} &= (1-v_{13}v_{31})/E_1, \quad a_{22} = (1-v_{23}v_{32})/E_2\\ a_{12} &= -(v_{12}+v_{23}v_{32})/E_1, \quad a_{66} = 1/G_{12}\end{aligned}\right\} \tag{8}$$

At plane stress, v_{13}, v_{31}, v_{23}, v_{32} are set to zero in Eq. (8).

The fomulas which map stress and displacement components into curvilinear coordinates (ξ, η) are shown:

$$\left.\begin{aligned}\sigma_\xi+\sigma_\eta &= \sigma_x+\sigma_y\\ \sigma_\eta-\sigma_\xi+2i\tau_{\xi\eta} &= e^{2i\phi}(\sigma_y-\sigma_x+2i\tau_{xy})\\ u_\xi-iu_\eta &= e^{i\phi}(u_x-iu_y)\end{aligned}\right\} \tag{9}$$

where

$$e^{i\phi} = \frac{\zeta}{|\zeta|}\frac{\omega'(\zeta)}{|\omega'(\zeta)|}, \quad e^{2i\phi} = \frac{\zeta}{\bar{\zeta}}\frac{\omega'(\zeta)}{\bar{\omega}'(\bar{\zeta})} \tag{10}$$

$$\left.\begin{aligned}z &= x+iy = \omega(\zeta) = R_0(\zeta+m/\zeta)\\ R_0 &= (a+b)/2, \quad m = (a-b)/(a+b)\end{aligned}\right\} \tag{11}$$

a and b represent the radii of the ellipse. Therefore, we may set $a=b$ (i.e., $m=0$) for the problem of the circular disk. Addtionally, the upper bars of the terms represent complex conjugates.

Now, we map into the following equation with ζ_k for complex variables z_k ($=x+\mu_k y$):

$$z_k = \omega_k(\zeta_k) = \frac{1}{2}\{(a - i\mu_k b)\zeta_k + (a + i\mu_k b)\zeta_k^{-1}\} \tag{12}$$

Through this procedure, the boundary and outer or inner region on the z_k-plane are mapped through a one-to-one correspondence into a unit circle and an outer or inner region on the ζ_k-plane.

3. Formulation of the problem

3.1. Solution for circular plane

One purpose of this paper is to obtain the solution for a problem in which diametrical concentrated load to an orthotropic elastic circular plane is applied, as shown in Fig. 2. We obtain the solution for this problem by the following procedure. First, tractions on the outer boundary Γ_0 of the elliptic plane with radii a_0, b_0, as shown in Fig. 3, are expanded into finite Fourier expansions,

$$\left.\begin{aligned} -\int_0^s Y_{n,0}ds &= \alpha_{0,0} + \sum_{m=1}^{M}(\alpha_{m,0}e^{im\theta} + \bar{\alpha}_{m,0}e^{-im\theta}), \\ \int_0^s X_{n,0}ds &= \beta_{0,0} + \sum_{m=1}^{M}(\beta_{m,0}e^{im\theta} + \bar{\beta}_{m,0}e^{-im\theta}) \end{aligned}\right\} \tag{13}$$

where, subscript 0 indicates the outer boundary.

The distance c from the origin to the focus is

$$c = \sqrt{a_1^2 - b_1^2} = \sqrt{a_0^2 - b_0^2} \tag{14}$$

Stress functions for the elliptic plane are expanded as follows

$$\Phi_1(z_1) = \sum_{m=1}^{M} A_{m,0}P_{1m}(z_1), \quad \Phi_2(z_2) = \sum_{m=1}^{M} B_{m,0}P_{2m}(z_2) \tag{15}$$

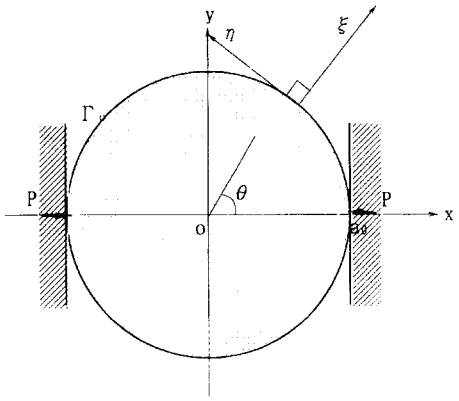

Fig. 2 Circular disk under diametral compression

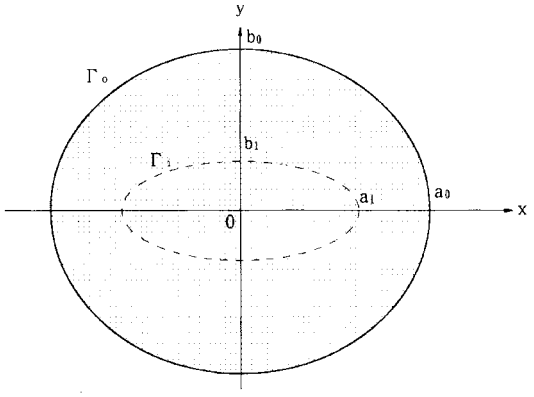

Fig. 3 Elliptic disk in the z-plane

Where $P_{km}(z_k)$ (k=1, 2) are the power series of m-th order for z_k, and are represented by ζ_k:

$$P_{km}(z_k) = -\{\zeta_k^m + (t_k\zeta_k^{-1})^m\} \tag{16}$$

where

$$t_k = \frac{a_0 + i\mu_k b_0}{a_0 - i\mu_k b_0} \quad (k = 1, 2) \tag{17}$$

If there is no rigid rotation, the complex coefficients $A_{m,0}$, $B_{m,0}$ must satisfy the following simultaneous equations:

$$\left.\begin{aligned}
&A_{1,0} + B_{1,0} + \bar{A}_{1,0} + \bar{B}_{1,0} = \frac{1}{a_0}(\alpha_{1,0} + \bar{\alpha}_{1,0}),\\
&\mu_1 A_{1,0} + \mu_2 B_{1,0} + \bar{\mu}_1\bar{A}_{1,0} + \bar{\mu}_2\bar{B}_{1,0}\\
&= \frac{1}{ib_0}(\bar{\alpha}_{1,0} - \alpha_{1,0}) = \frac{1}{a_0}(\beta_{1,0} + \bar{\beta}_{1,0}),\\
&\mu_1^2 A_{1,0} + \mu_2^2 B_{1,0} + \bar{\mu}_1^2\bar{A}_{1,0} + \bar{\mu}_2^2\bar{B}_{1,0}\\
&= \frac{1}{ib_0}(\bar{\beta}_{1,0} - \beta_{1,0}),\\
&(q_1 - \mu_1 p_1)A_{1,0} + (q_2 - \mu_2 p_2)B_{1,0}\\
&+(\bar{q}_1 - \bar{\mu}_1\bar{p}_1)\bar{A}_{1,0} + (\bar{q}_2 - \bar{\mu}_2\bar{p}_2)\bar{B}_{1,0} = 0
\end{aligned}\right\} \tag{18}$$

$$\left.\begin{aligned}
&A_{m,0} + B_{m,0} + \bar{t}_1^m\bar{A}_{m,0} + \bar{t}_2^m\bar{B}_{m,0} = -\alpha_{m,0}\\
&\mu_1 A_{m,0} + \mu_2 B_{m,0} + \bar{\mu}_1\bar{t}_1^m\bar{a}_{m,0} + \bar{\mu}_2\bar{t}_2^m\bar{B}_{m,0} = -\beta_{m,0}\\
&t_1^m A_{m,0} + t_2^m B_{m,0} + \bar{A}_{m,0} + \bar{B}_{m,0} = -\bar{\alpha}_{m,0}\\
&\mu_1 t_1^m A_{m,0} + \mu_2 t_2^m B_{m,0} + \bar{\mu}_1\bar{A}_{m,0} + \bar{\mu}_2\bar{B}_{m,0} = -\bar{\beta}_{m,0}\\
&(m \geq 2)
\end{aligned}\right\} \tag{19}$$

Now, we may set a_0=b_0 for the problem of circular planes. Solving these equations, $A_{m,0}$, $B_{m,0}$ can be determined.

3.2. Solution for circular ring

Another purpose of this paper is to obtain the solution for a problem in which diametrical concentrated load is applied to an orthotropic elastic circular ring. In this section, the solution for orthotropic elastic circular rings is shown, superposing solutions for an infinite plane with a circular opening, and the circular plane explained in the previous section. First, the coordinates corresponding to the inner virtual boundary Γ_0 in the elliptic plane explained in the previous section are

$$x_1 = a_1\cos\theta, \quad y_1 = b_1\sin\theta \tag{20}$$

Because the outer and inner boundaries are confocal ellipses, Eq. (14) must be satisfied.

Using z_k-coordinates

$$z_{k,1} = x_1 + \mu_k y_1 \quad (k = 1, 2) \tag{21}$$

the resultant forces on Γ can be determined by

$$\left.\begin{aligned} -\int_0^s \tilde{Y}_{n,1} ds &= 2Re[\Phi_1(z_{1,1}) + \Phi_2(z_{2,1})] \\ \int_0^s \tilde{X}_{n,1} ds &= 2Re[\mu_1 \Phi_1(z_{1,1}) + \mu_2 \Phi_2(z_{2,1})] \end{aligned}\right\} \tag{22}$$

The right sides of the above equations are expanded into Fourier expansions:

$$\left.\begin{aligned} -\int_0^s \tilde{Y}_{n,1} ds &= \gamma_{0,1} + \sum_{m=1}^{M} (\gamma_{m,1} e^{im\theta} + \overline{\gamma}_{m,1} e^{-im\theta}) \\ \int_0^s \tilde{X}_{n,1} ds &= \varepsilon_{0,1} + \sum_{m=1}^{M} (\varepsilon_{m,1} e^{im\theta} + \overline{\varepsilon}_{m,1} e^{-im\theta}) \end{aligned}\right\} \tag{23}$$

Secondly, consider an infinite plane with an elliptic opening with radii a_1, b_1 under loading for cancelling out the resultant force on the inner boundary Γ_i of the elliptic ring, as shown in Fig. 5.

In this case, the stress functions are represented by the following equations:

$$\Phi_1(z_1) = \sum_{m=1}^{M} C_{m,1} \zeta_1^{-m}, \quad \Phi_2(z_2) = \sum_{m=1}^{M} D_{m,1} \zeta_2^{-m} \tag{24}$$

where

$$C_{m,1} = -\frac{1}{\mu_1 - \mu_2}(\overline{\varepsilon}_{m,1} - \mu_2 \overline{\gamma}_{m,1}), \qquad D_{m,1} = \frac{1}{\mu_1 - \mu_2}(\overline{\varepsilon}_{m,1} - \mu_1 \overline{\gamma}_{m,1}) \tag{25}$$

$$\zeta_k = \frac{1}{a_1 - i\mu_k b_1}(z_k \pm \sqrt{z_k^2 - a_1^2 - \mu_k^2 b_1^2}) \tag{26}$$

We may set a_1=b_1 for the problem under consideration. The coodinates corresponding to the outer virtual boundary Γ_o, shown by the broken line in Fig. 5, are represented by the following equations:

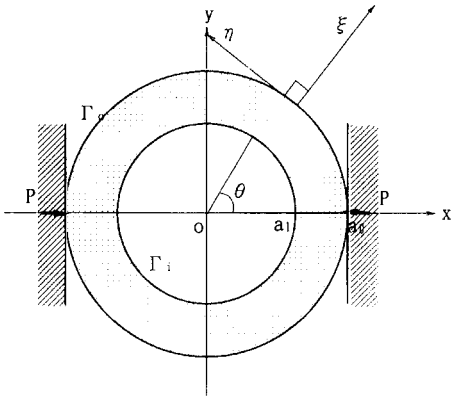

Fig. 4 Circular ring under diametral compression

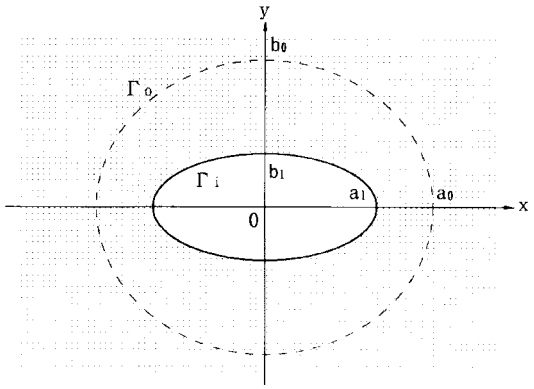

Fig. 5 Infinite plate with elliptic hole in the z-plane

$$x_0 = a_0 \cos\theta, \quad y_0 = b_0 \sin\theta \tag{27}$$

Using the z_k-plane,

$$z_{k,0} = x_0 + \mu_k y_0 \tag{28}$$

Therefore, the resultant force on the boundary Γ_0 is represented as

$$\left.\begin{aligned} \int_0^s Y_{n,1} ds &= 2Re[\Phi_1(z_{1,0}) + \Phi_2(z_{2,0})] \\ -\int_0^s X_{n,1} ds &= 2Re[\mu_1 \Phi_1(z_{1,0}) + \mu_2 \Phi_2(z_{2,0})] \end{aligned}\right\} \tag{29}$$

The same holds for the inner boundary, with the right side of the above equations expanded into Fourier expansions:

$$\left.\begin{aligned} \int_0^s Y_{n,1} ds &= \alpha_{0,1} + \sum_{m=1}^{M} (\alpha_{m,1} e^{im\theta} + \bar{\alpha}_{m,1} e^{-im\theta}) \\ -\int_0^s X_{n;1} ds &= \beta_{0,1} + \sum_{m=1}^{M} (\beta_{m,1} e^{im\theta} + \bar{\beta}_{m,1} e^{-im\theta}) \end{aligned}\right\} \tag{30}$$

To cancel out the resultant force on the outer virtual boundary Γ_o in the finite plane with an elliptic opening, the negative values of the above resultant forces are loaded on the boundary of the elliptic plane shown in Fig. 3. In the following procedure the above operation is repeated N times to satisfy both boundary conditions. As a result, the stress functions for the orthotropic elliptic ring are obtained by

$$\left.\begin{aligned} \Phi_1(z_1) &= \sum_{m=1}^{M} (\hat{A}_m^N P_{1m}((z_1) + \hat{C}_m^N \zeta_1^{-m})) \\ \Phi_2(z_2) &= \sum_{m=1}^{M} (\hat{B}_m^N P_{2m}(z_2) + \hat{D}_m^N \zeta_2^{-m}) \end{aligned}\right\} \tag{31}$$

where

$$\left.\begin{aligned} \hat{A}_m^N &= \sum_{n=0}^{N} A_{m,n}, \quad \hat{B}_m^N = \sum_{n=0}^{N} B_{m,n} \\ \hat{C}_m^N &= \sum_{n=1}^{N} C_{m,n}, \quad \hat{D}_m^N = \sum_{n=1}^{N} D_{m,n} \end{aligned}\right\} \tag{32}$$

The coefficients in the above equations are obtained, for example, as Eq. (25).

3.3. Applied load

We address the problem of orthotropic circular planes or circular rings under diametrical loadings

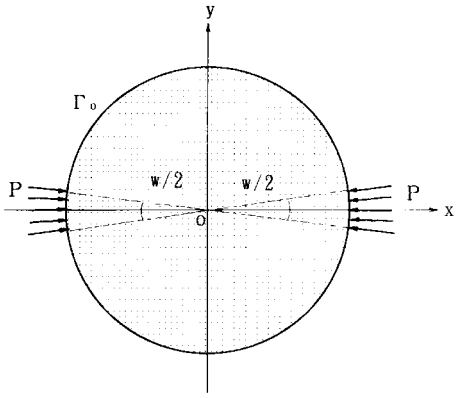

Fig. 6 Schematic diagram of the diametral compression test

in this paper. If the boundary conditions are given as resultant forces, the equations are the following:

$$\left.\begin{aligned} \int_0^s X_n ds &= \begin{cases} -P, & 0 \le \theta < \pi \\ 0, & \pi \le \theta < 2\pi \end{cases} \\ -\int_0^s Y_n ds &= 0 \end{aligned}\right\} \tag{33}$$

In this case, the coefficients α_m, β_m (m≥1) are given as

$$\beta_m = \frac{iP}{2m\pi}\{1-(-1)^m\},\ \alpha_m = 0 \tag{34}$$

We represent the concentrated force as loading on a point on the boundary. To approximate this condition, consider the circular plane or circular ring loaded to the width ω/2(*rad*) and the magnitude P, of which the center is on the x-axis. The resultant forces on the boundaries are represented by

$$\left.\begin{aligned} \int_0^s X_n ds &= \begin{cases} -\dfrac{2P\theta}{w}, & -\dfrac{w}{4} \le \theta \le \dfrac{w}{4} \\ -\dfrac{P}{2}, & \dfrac{w}{4} \le \theta \le \pi - \dfrac{w}{4} \\ -\dfrac{P}{2} + \dfrac{2P}{w}\left(\theta - \pi + \dfrac{w}{4}\right) & \\ \pi - \dfrac{w}{4} \le \theta \le \pi + \dfrac{w}{4} & \\ \dfrac{P}{2}, \ \pi + \dfrac{w}{4} \le \theta \le 2\pi - \dfrac{w}{4} & \end{cases} \\ -\int_0^s Y_n ds &= 0 \end{aligned}\right\} \tag{35}$$

where

$$\beta_m = -\frac{2iP}{\pi m^2 \omega}\{1-(-1)^m\}\sin\frac{m\omega}{4}, \quad \alpha_m = 0 \tag{36}$$

4. Results and discussion

4.1. Circular plane

Fig. 7 shows how the normalized tensile stress ($\sigma_{y0}/\sigma_{yiso}$) on the x-axis of the circular plane is affected by the load area for the selected orthotropy ratio (E_2/E_1=2.0, 5.0) and the angle between the principal material direction and coordinate axis (Ψ=0, π/4, π/2).

In analysis using a series as in the present study, the convergence and accuracy of calculated value must be always discussed. The number of terms M in Eq. (13) affects this. It is not neccesary to use a large number of terms to calculate in the case of large loading areas. Nevertheless, A_n, B_n converge to zero using one hundred terms; little change is observed using larger number of terms at $\omega/2\pi = 2\%$. On the other hand, a large number of terms is necessary for problems involving concentrated force, because the resultant forces are represented as step functions. A_n, B_n converge to zero with two hundred fifty terms. The error is 6% with one hundred terms, 3% with 150 terms and 1% with two hundred terms. In this paper, calculations were carried out with 250 terms for concentrated force, otherwise one hundred terms.

For E_2/E_1=2.0, the minimum value is observed at the center of the circular plane, and the maximum value at a distance of 0.9 times the radius from the center of the circular the plane when the principal material directions are parallel to the axes (i.e., $\Psi = 0$, π/2).

Furthermore, there is good agreement between the authors' numerical results and the numerical results from FEM obtained by Lemmon *et al.* (1996) on load area $\omega/2\pi = 2\%$, 4%, 8% for the circular plane. Conversely, maximum value is observed at the center of the circular plane when the principal material direction is not parallel to the axes (i.e., $\Psi = \pi/4$). For E_2/E_1=5.0, the minimum value at the center of the circular plane decreases; the maximum value at a distance of 0.9 times the radius from the center of the circular plane increases when the principal material directions are parallel to the axes. In addition, the maximum value is observed at a distance of 0.95 times the

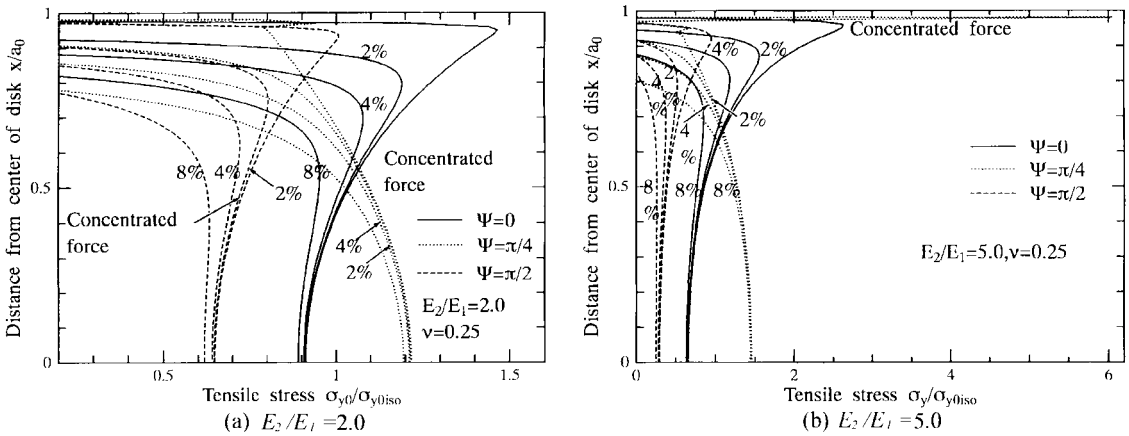

(a) E_2/E_1=2.0 (b) E_2/E_1=5.0

Fig. 7 The effect of loading area on tensile stress along the diameter

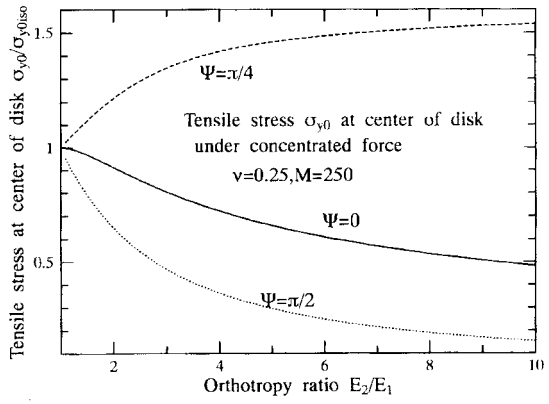

Fig. 8 The effect of orthotropic elastic ratio on tensile stress at the center of disk

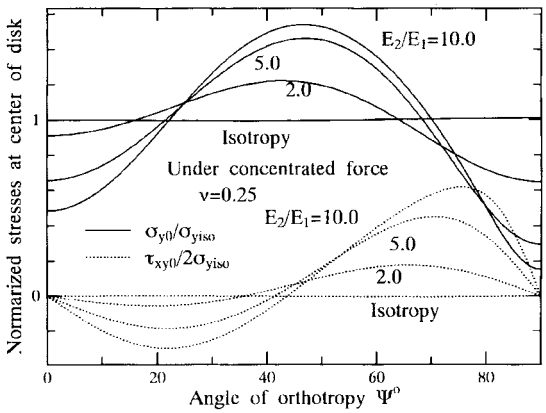

Fig. 9 The effect of angle of orthotropy on stresses at the center of disk

radius from the center of the circular plane when concentrated forces are loaded on the circular plane, of which the principal material directions incline $\pi/4$ to the axes.

Fig. 8 shows the dependence of the normalized tensile stresses at the center of the circular plane ($\sigma_{y0}/\sigma_{yiso}$) as a function of the material orthotropy ratio. The graph shows the stress at the center of the circular plane for cases in which the principal material directions are parallel to the axes (Ψ=0, $\pi/2$) and for those that are not parallel ($\Psi=\pi/4$). Tensile stresses decrease as the material orthotropy ratio increases when the principal material directions are parallel to the axes; however, tensile stresses increase as the material orthotropy ratio increases when the principal material directions are not parallel to the axes.

Fig. 9 shows the normarized tensile stress (σ_y/σ_{yiso}) and shear stress ($\tau_{xy}/(2\sigma_{yiso})$) at the center of the circular plane as a function of the material orientation (Ψ in degree) for four selected material orthotropy ratios (E_2/E_1=0.98(*Isotropy*), 2.0, 5.0, 10.0) under concentrated force. The shear stress at the center of the circular plane is zero when the principal material directions are parallel to the axes (i.e., Ψ=0°, 90°), but is otherwise nonzero.

Fig. 9 also shows that as the orthotropy ratios increase, the magnitudes of both the tensile and shear stresses increase and are greater than that of the isotropic case.

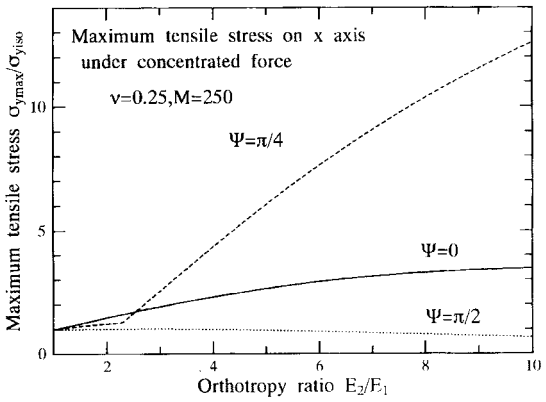

Fig. 10 The effect of orthotropic elastic ratio on maximum tensile stress

Fig. 10 shows the dependance of the normalized maximum tensile stress ($\sigma_{ymax}/\sigma_{yiso}$) as a function of the material orthotropy ratio. The graph shows that the maximum tensile stress on the x-axis increases asymptotically to 3.5 when $\Psi=0$, and decreases when $\Psi=\pi/2$. When the principal material directions are not parallel to the axes (i.e., $\Psi=\pi/4$), the maximum tensile stress is not smooth at $E_2/E_1=2.3$. Therefore, maximum tensile stress appears on the center of the circular plane when the

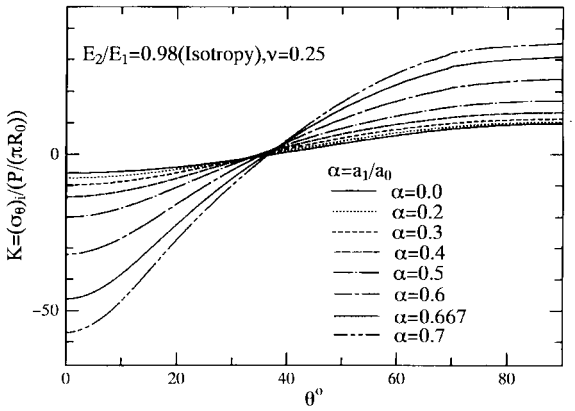

(a) Stress factors at the inner boundary

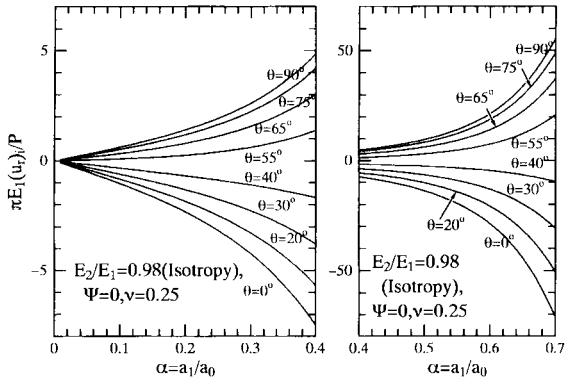

(b) Radial displacements along the inner boundary

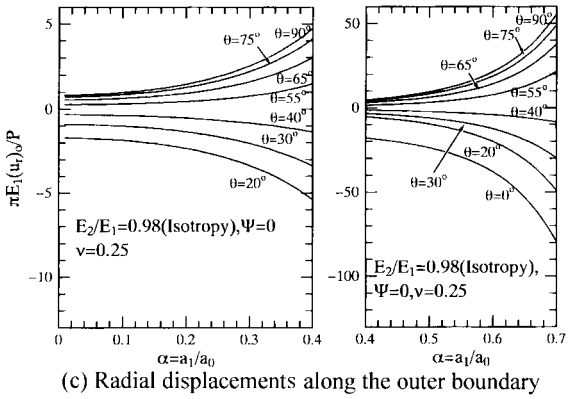

(c) Radial displacements along the outer boundary

Fig. 11 Stresses and displacements on the boundaries of isotropic circular ring under diametral compression

orthotropy ratio is smaller than 2.3 and at a distance of 0.95 times the radius from the center of the circular plane when the orthotropy ratio is larger than 2.3.

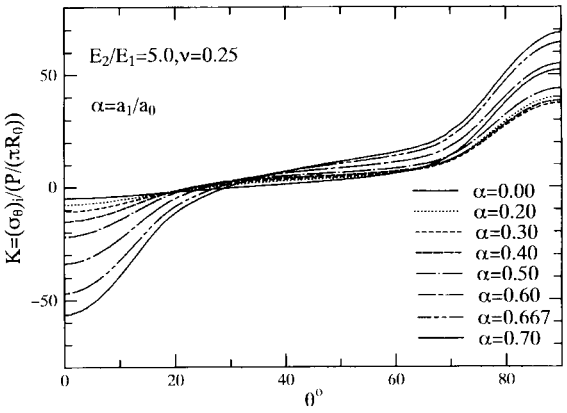

(a) Stress factors at the inner boundary

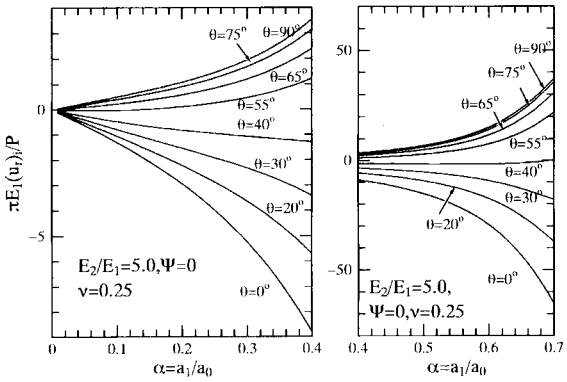

(b) Radial displacements along the inner boundary

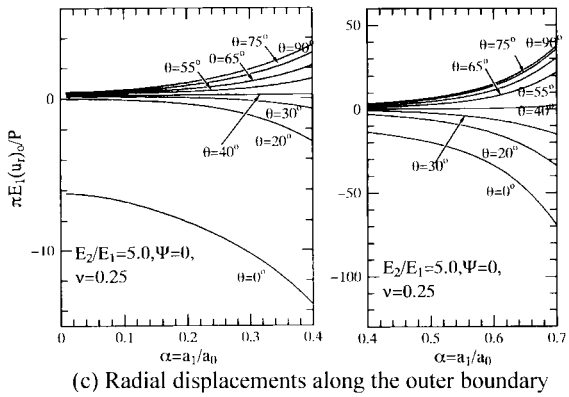

(c) Radial displacements along the outer boundary

Fig. 12 Stresses and displacements on the boundaries of orthotropic (E_2/E_1=5.0) circular ring under diametral compression

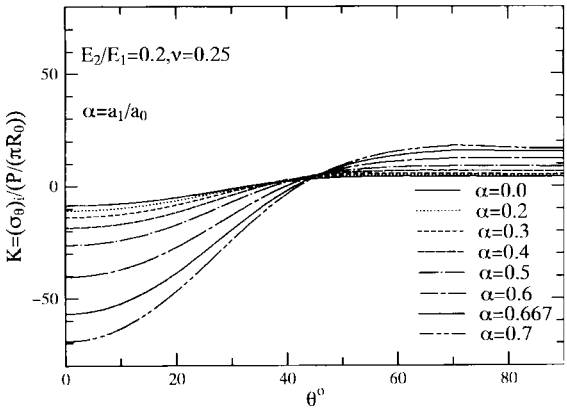

(a) Stress factors at the inner boundary

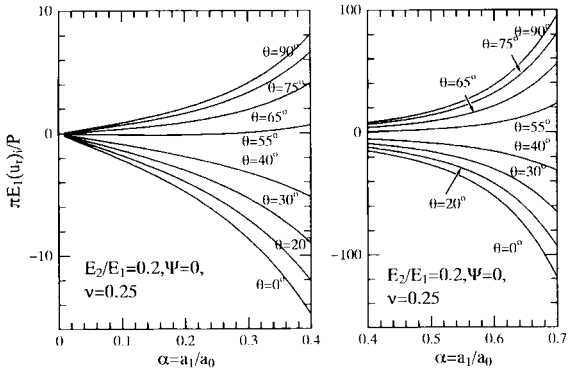

(b) Radial displacements along the inner boundary

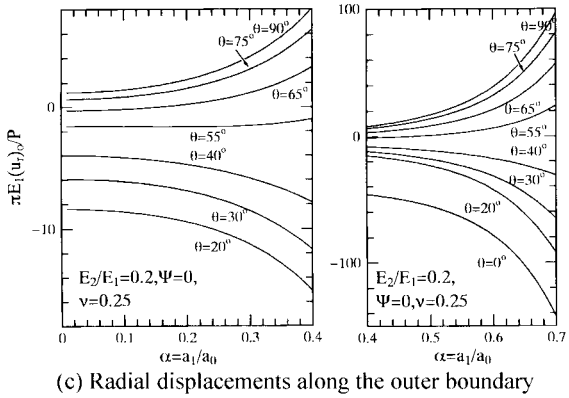

(c) Radial displacements along the outer boundary

Fig. 13 Stresses and displacements on the boundaries of orthotropic (E_2/E_1=0.2) circular rings under diametral compression

4.2. Circular ring

(a), (b) and (c) in Fig. 11 show the normalized tangential stresses, normal displacements on the inner boundary and normalized normal displacements on the outer boundary for the isotropic circular ring, where $\alpha=a_0/a_1$ is the parameter representing the thickness of the circular ring. In this study, the accuracy of the analysis depends on the accuracy of estimating the resultant force on both boundaries, because of the cancelling out of the resultant force arising on the virtual boundary of the circular plane or on the infinite plane with a circular opening. And the greater accuracy of convergences of Eqs. (23) and (25) becomes slower as the more thickness of circular ring decreases. Calculation is carried out when the number of terms is 250 through the thickness of the circular ring.

Furthermore, the number of repeated calculations N increases as the thickness of circular ring α increases. In this study, N is a value from 5 to 50. Except for the displacement on the loading point, there is good agreement between the computations here and those shown by Nelson or Durelli *et al.* when α is smaller than 0.7. When α is greater than 0.7, the present authors' numerical results are smaller than those reported by Durelli, in the case of a large enough value of N. Further, the difference between the authors' numerical results and those of Durelli become greater as α increases.

It is observed that tangential stress, normal stress on the inner boundary, and normal displacement on the outer boundary increase with the thickness of circular ring.

Fig. 12 and Fig. 13 show graphs similar to those in Fig. 11 for an orthotropic elliptic circular ring. For both of these, the principal material directions are parallel to the axes; Fig. 12 is for $E_2/E_1=5.0$, and Fig. 13 is for $E_2/E_1=0.2$. It is observed that the normal stress at $\theta=90^0$ on the inner boundary is larger and the displacement is smaller than that of an isotropic circular ring when Young's modulus parallel to loading is larger, and the reverse is true when Young's modulus parallel to loading is smaller.

5. Conclusions

In this paper, solutions are proposed for orthotropic elastic circular planes under diametrical loading with Lekhnitskii's complex variable. The applicability of the analytical solutions in this paper has been evaluated with reference to the numerical results of FEM.

Furthermore, solutions are proposed for orthotropic elastic circular rings under diametrical loading by superposing the solutions proposed in this paper and the solutions for orthotropic elastic infinite planes with a circular opening proposed by Lekhnitskii (1968) for the required boundary conditions. For isotropic elastic circular rings, there is good agreement between the authors' numerical results and those of Durelli *et al.* (1986) or Nelson (1939). For orthotropic elastic circular rings, some numerical results are shown in this paper.

References

Cauweleart, F.V. and Eckmann, B. (1994), "Indirect tensile test applied to anisotropic materials", *Materials and Structures*, **27**, 54-60.

Durelli, A.J. and Lin, Y.H. (1986), "Stresses and displacements on the boundaries of circular rings diametrically

loaded", *Jour. Appl. Mech.*, **53**, 213-219.
Hayashi, T. (1960), "On the plane stress problem in a ring of orthogonally aeolotropic material", (in Japanese), *Trans. of JSME Series 1*, **26**(164), 516-523.
Hetenyi, M. (1960), "A method of solution for the elastic quarter-plane", *Jour. Appl. Mech.*, **27**, 289-296.
Kawakubo, S., Tsutsumi, T. and Hirashima, K. (1996), "Stress and displacement fields for an anisotropic elliptical disk subjected to arbitrary loads at the boundary" (in Japanese), *Trans. of JSME Series A*, **62**(599), 1626-1633.
Kawamoto, T. (1968), *Applied Elasticity* (in Japanese), Kyoritsu Pub.
Lekhnitskii, S.G. (1968), *Anisotropic Plate*, Gordon & Breach.
Lemmon, R.K. and Blackketter, D.M. (1996), "Stress analysis of an orthotropic material under diametral compression", *Exp. Mech.*, **36**, 204-211.
Moriguchi, S. (1957), *Two Dimensional Elasticity*, (in Japanese), Iwanami Pub.
Nelson, C.W. (1939), "Stresses and displacements in a hollow circular cylinder", Ph.D thesis, University of Michigan.
Tsutsumi, T. and Hirashima, K. (1997), "Analysis of anisotropic elliptic ring by using constraint release technique" (in Japanese), *Trans. of JSME Series A*, **63**(615), 2411-2416.